RSC Advances



This is an *Accepted Manuscript*, which has been through the Royal Society of Chemistry peer review process and has been accepted for publication.

Accepted Manuscripts are published online shortly after acceptance, before technical editing, formatting and proof reading. Using this free service, authors can make their results available to the community, in citable form, before we publish the edited article. This Accepted Manuscript will be replaced by the edited, formatted and paginated article as soon as this is available.

You can find more information about *Accepted Manuscripts* in the **Information for Authors**.

Please note that technical editing may introduce minor changes to the text and/or graphics, which may alter content. The journal's standard <u>Terms & Conditions</u> and the <u>Ethical guidelines</u> still apply. In no event shall the Royal Society of Chemistry be held responsible for any errors or omissions in this *Accepted Manuscript* or any consequences arising from the use of any information it contains.



Preparation of NaLuF₄: Gd, Yb, Tm/TiO₂ Nanocomposite with High Catalytic Activity for Solar Light Assisted Photocatalytic Degradation of Dyes and Wastewater

Chengcheng Wang^a, Kailin Song^a, Yi Feng^b, Dongguang Yin^{a*}, Juan Ouyang^a, Bing Liu^a, Xianzhang Cao^a, Lu Zhang^a, Yanlin Han^a, Minghong Wu^{a*}

^aSchool of Environmental and Chemical Engineering, Shanghai University, Shanghai 200444, China

^bMetal Health Center of Shanghai Zhabei District, Shanghai, 200436,China

Noted: Chengcheng Wang, Kailin Song and Yi Feng are co-first author

ABSTRACT: A new nanocomposite NaLuF₄: Gd, Yb, Tm/TiO₂ photocatalyst was developed. Its morphology, size, crystalline phase, composition, absorbance and emission spectra were characterized by X-ray diffraction, transmission electron microscopy, energy-dispersive X-ray analysis, ultraviolet-visible absorbance spectra and fluorescence spectra, respectively. The photocatalytic degradation of dyes including rhodamine B (RhB), methyl blue (MB) and methyl orange (MO), dye mixture and dye wastewater under the simulated solar light irradiation were evaluated. The degradation ratios and the removal rations of chemical oxygen demand (COD) of the dyes and dye wastewater after the photo-degradation were measured. The results show that the as-prepared nanocomposite exhibits high photocatalytic activity, and it can not only efficiently degrade single dye, but also mixture and dye wastewater.

KEYWORDS: NaLuF₄: Gd, Yb, Tm /TiO₂ Nanocomposite; Photocatalysis; Synthesis; Solar

Light; Photocatalytic Activity

1. Introduction

As the increase of the amount of wastewater containing poisonous organic compounds generated, dye wastewater pollution has become a big challenge all over the world, ^{1,2} Dye molecules usually contains one or several benzene rings which are hard to be degraded by traditionally chemical and biological methods. Photocatalysis is an effective and environmentally friend technique for the degration of toxic organic substances in air and water. Especially, clean, safe and renewable solar energy can be used to fulfill this purpose. ^{2,3} TiO₂, due to its high catalytic activity, physical and chemical stabilities, non-toxicity and low-cost, has been widely studied on the degradation of organic pollutions. 4-6 However, due to the large bandgap of TiO₂ (~3.2eV), it can only harvest UV light. Considering that the percentage of UV light in the solar spectrum is only 5%, which is much lower than that in visible (~ 49%) and near-infrared (NIR) region (~ 46%), 7-8 the overall energy harvesting efficiency of TiO₂ is quite low. Up to now, many methods have been adopted to extend the absorption of TiO₂ into visible light region, e.g. surface modification, doping of metallic and nonmetallic elements. 9-12 Although the absorption spectra of TiO₂ was effectively expanded, the overall catalytic efficiency was not substantially improved. Potential reasons might be the oxidation-reduction potentials of electron-hole pairs that generated by the excitation of long wavelength lights is too small to catalyze the reacion. ^{7,8,13} Only those holes produced from the excitation of ultraviolet lights possess enough oxidative ability to degrade organic pollutants. Thus, although the absorption range of TiO_2 is extended to visible lights, it is difficult to obtain the higher degradation efficiency. ^{14,15} Moreover, the large fraction in NIR light remains unexplored.

In recently years, some studies shown that the construction of upconversion nanoparticles and TiO_2 nanocomposite is a good approach to improve NIR light harvesting efficiency and photocatalytic activity of TiO_2 . 13,16,17 The upconversion material upconvert NIR (or visible light) into high-energy UV light, which can be absorbed by TiO_2 . 14,16,18 This method can not only extend the light response range of TiO_2 into NIR (or visible light), but also excite the TiO_2 by UV light supplied from upconversion materials. The integration of upconversion materials and TiO_2 presents an ideal strategy to improve the photocatalytic efficiency of TiO_2 based catalysts.

To date, numerous of fluoride-based host matrixs and upconversion materials have been developed. Among these materials, NaLuF₄ has been proved to be a good host material. Our previous study found that NaLuF₄: Yb/Tm and NaLuF₄: Gd/Yb/Er displayed higher upconversion luminescence efficiency in comparison to the counterparts of NaYF₄-based nanocrystals.¹⁹ Li's group reported that lanthanide doped NaLuF₄ nanocrystals with size of 7.8 nm were more efficient than NaYF₄-based nanocrystals as well, and it was demonstrated to be a good biomarker for in vivo bioimaging.²⁰ Qin's group found that β-NaLuF₄:Yb, Tm showed intense ultraviolet and blue upconversion emission with longer fluorescence lifetime compared with NaYF₄-based one.²¹ Although NaLuF₄ is an excellent host for upconversion luminescence, the study of using NaLuF₄-based upconversion materials as spectrum modifier

for TiO₂ has not been reported.

In this study, we prepared a new photocatalyst of nanocomposite NaLuF₄: Gd, Yb, Tm/TiO₂ and investigated its photocatalytic property. Improved photocatalytic efficiency was shown. ^{15, 22,23} To the best of our knowledge, this is the first time to study the nanocomposite NaLuF₄: Gd, Yb, Tm/TiO₂ for solar light assisted photocatalytic degradation of dye and wastewater.

2. Experimental

2.1. Materials

Rare earth oxides of Lu₂O₃ (99.999%), Gd₂O₃ (99.999%), Yb₂O₃ (99.999%), and Tm₂O₃ (99.999%) were purchased from Shanghai Yuelong New Materials Co. Ltd. Oleic acid (OA) (>90%), 1-octadecene (>90%) and thioglycollic acid (TGA) (>98%) were purchased from Sigma-Aldrich. Titanium (IV) ethoxide (>98%), NaOH, NH₄F, hydrochloric acid, RhB, MB, MO, ethanol, methanol and cyclohexane were purchased from Sinopharm Chemical Reagent Co., Ltd. (Shanghai). The dye wastewater was supplied from Shanghai Jinshan Langxia silk carpet Co. Ltd.. P25 (TiO₂, 99.5%) was purchased from Degussa Co. Ltd.(Germany). LnCl₃ (Ln: Lu, Gd, Yb, Tm) were prepared by dissolving the corresponding metal oxides in hydrochloric acid at elevated temperature.

2.2. Synthesis of NaLuF₄: Gd, Yb, Tm upcovnersion nanocrystals

For synthesizing NaLuF₄: Gd, Yb, Tm nanocrystals, 0.555 mmol of LuCl₃, 0.24 mmol of GdCl₃, 0.20 mmol of YbCl₃, and 0.005 mmol of TmCl₃ were mixed with 6 mL oleic acid (OA) and 15 mL octadecene (ODE) in 50 mL three-necked flask under stirring. The solution was heated to 160 °C and kept for 30 min, then cooled down to room temperature. Subsequently, 10 mL methanol solution containing NaOH (4 mmol) and NH₄F (2.5 mmol) were slowly added into the flask and kept for 30 min. The solution was heated to 100 °C and kept for 30 min to remove methanol and water, then heated to 310 °C under nitrogen atmosphere and kept for 1h. After the solution was cooled down to room temperature, nanocrystals were precipitated from the solution with ethanol, and collected after centrifuging and washing with ethanol/water (1:1 v/v) for three times.

2.3. Synthesis of hydrophilic NaLuF₄: Gd, Yb, Tm upconversion nanocrystals

The above prepared NaLuF₄: Gd, Yb, Tm upconversion nanocrystals are hydrophobic. In order to synthesize NaLuF₄: Gd, Yb, Tm/TiO₂ nanocomposite, it need to be converted to hydrophilic nanocrystals firstly. In a typical experiment, 1.0 mmol of prepared NaLuF₄: Gd, Yb, Tm nanocrystals dissolved in 25 mL of cyclohexane was added to 50 mL of ethanol containing 5 mL of TGA and stirred for 48 h at room temperature. Then the nanocrystals were isolated by centrifugation, washed several times with deionized water and ethanol, and then redispersed in ethanol.

2.4. Synthesis of NaLuF₄: Gd, Yb, Tm/TiO₂ nanocomposite

0.25 mmol of hydrophilic NaLuF₄: Gd, Yb, Tm nanocrystals were dispersed in 20 mL ethanol and stirred for 30 min. 100 μ L Titanium (IV) ethoxide dispersed in 40 mL ethanol was added to the solution under ultrasound for 2 h at room temperature. Then 20 mL ethanol containing 1.5 mmol deionized water was added into the mixture drop by drop. The above precursor solution was transferred to a 100 mL autoclave, sealed, and maintained at 160 $^{\circ}$ C for 20 h. The final products were collected by centrifugation and washed with deionized water and ethanol several times, and then dried at 60 $^{\circ}$ C in air.

For preparation of NaLuF₄: Gd, Yb,Tm-TiO₂ physical mixture, the NaLuF₄: Gd, Yb, Tm and TiO₂ were synthesized according to the above procedure first, then they were mixed mechanically in the same ratio of NaLuF₄: Gd, Yb, Tm and TiO₂ as that of the NaLuF₄: Gd, Yb, Tm/TiO₂ nanocomposite.

2.5. Characterization

X-ray powder diffraction (XRD) measurements were performed on a Rigaku D/max-2500 X-ray diffractometer using Cu K α radiation. Transmission electron microscopy (TEM) analyses were performed on a JEOL JEM-2010F electron microscope operating at 200 kV. Energy-dispersive X-ray analysis (EDX) of the samples was performed during high-resolution transmission electron microscopy (HRTEM) measurements. UV-vis-NIR absorption spectra were measured on a Hitachi 3010 UV-vis spectrophotometer (Japan). The upconversion fluorescence emission spectra were recorded with an Edinburgh FLS-920 fluorescence spectrometer by using an external 0-2W adjustable laser (980 nm, Beijing Hi-Tech Optoelectronic Co., China) as the excitation source instead of the Xenon source in the spectrophotometer.

2.6. Photocatalytic Experiments

Photocatalysis was performed via monitoring RhB degradation by measuring the variation of optical absorption of RhB with a Hitachi U-3010 spectrophotometer, using SGY-IB multifunction of photochemical reactor (Nanjing Sidongke Electri Co. Ltd.) as photocatalytic reaction device. In a typical experiment, 20 mg of sample (catalyst) was dispersed into a quartz cuvette containing 50 mL of RhB aqueous solution (10 mg/L). The suspension was magnetically stirred in the dark for 30 min to attain adsorption— desorption equilibrium between dye and catalyst. Then the photoreaction vessels were exposed to the simulated solar light irradiation produced by a 500 W Xe lamp (PL-X500D) (the wavelength distribution is similar to the solar light). At giving time intervals, the photoreacted solutions were analyzed by recording variations of the absorption band maximum (554 nm) in the UV-Visible spectra of RhB.

The degradation ratio η (%) of dye was calculated using the following equation:

$$\eta$$
 (%) = [(C₀-C)]/C₀×100
= [(A₀-A)]/A₀×100

Where C_0 and C are the initial and residual concentrations of RhB in solution resepctively, and A_0 and A are the absorbance of RhB at 554nm before and after exposing under simulated solar light respectively.

In order to evaluate the extent of mineralization of dye by photocatalysis, the chemical oxygen demand (COD) of the dye was measured. The COD was determined by standard dichromate method.²⁴ The COD removal ratios (%) of dye was calculated using the following equation:

COD removal (%) =
$$[(COD_0 - COD)]/(COD_0 \times 100)$$

Where COD_0 and COD are the chemical oxygen demand values of dye solution before and after photocatalytic degradation.

3. Results and discussion

3.1. Phase and morphology characterization

Figure 1 shows the XRD patterns of the as-prepared products. The diffraction peaks of the NaLuF₄: Gd, Yb, Tm (Figure 1a) can be indexed as a typical pure hexagonal phase according to the JCPDS file NO. 27-0726. No impurity peaks can be identified from the XRD pattern, indicating the desired product of pure hexagonal-phase NaLuF₄: Gd, Yb, Tm nanocrystals are synthesized successfully. It can be seen from Figure 1 that the TiO₂ nanoparticles are amorphous before annealing (Figure 1b) and crystalline after hydorthermally annealling at 160°C for 20 h (Figure 1c). As shown in the XRD pattern of NaLuF₄: Gd, Yb, Tm/TiO₂ nanocomposite (Figure 1c), the characteristic diffraction peaks of TiO₂ are observed which are assigned to anatase titania according to the JCPDS file No. 21-1272, while NaLuF₄: Gd, Yb, Tm still maintains the pure hexagonal phase structure.

The TEM images of prepared products are shown in Figure 2. As shown in Figure 2a, NaLuF₄: Gd, Yb, Tm nanocrystals have hexagonal plate-liked structure with diameter about 45 nm, which are uniform and the nanocrystals are well-dispersed. The TEM images of nanocomposite NaLuF₄: Gd, Yb, Tm /TiO₂ show that a lot of small-sized (10 nm) nanoparticles of TiO₂ are dispersed around the NaLuF₄: Gd, Yb, Tm particles, where the size and shape of NaLuF₄: Gd, Yb, Tm particles remain the same. The HRTEM images of NaLuF₄: Gd, Yb, Tm (Figure 2a, inset) and TiO₂ (Figure 2b, inset) reveal highly crystalline natures of

the as-prepared products. The interplanar distances between adjacent lattice fringes correspond to the crystal planes of the nanocrystals, ^{23,25} agreeing with the XRD detected results. The composition of nanocomposite NaLuF₄: Gd, Yb, Tm/TiO₂ was characterized by EDX analysis. As shown in Figure 2c, almost all of the elements including Na, Lu, F, Gd, Yb, Ti, and O were detected, further confirmed the composition of the nanocomposite.

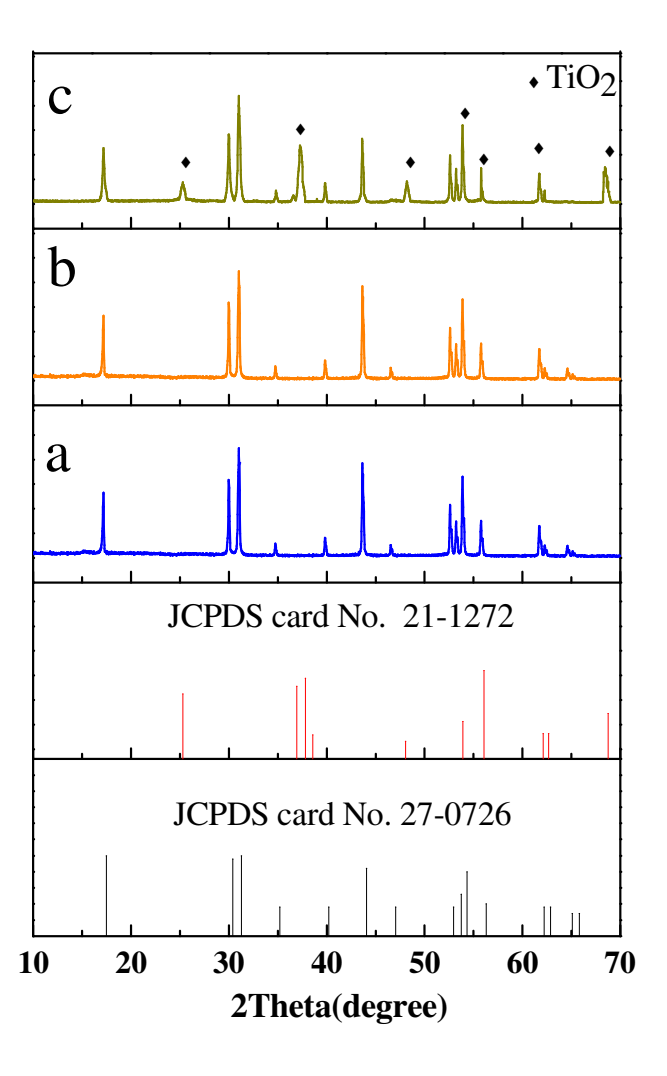


Figure 1. XRD patterns of NaLuF₄: Gd, Yb, Tm nanocrystal (a), NaLuF₄: Gd, Yb, Tm/TiO₂ nanocomposite before hydrothermally annealed (b) and after hydrothermally annealed (c). Standard XRD patterns of JCPDS card No. 27-0726 (NaLuF₄) and 21-1272 (TiO₂).

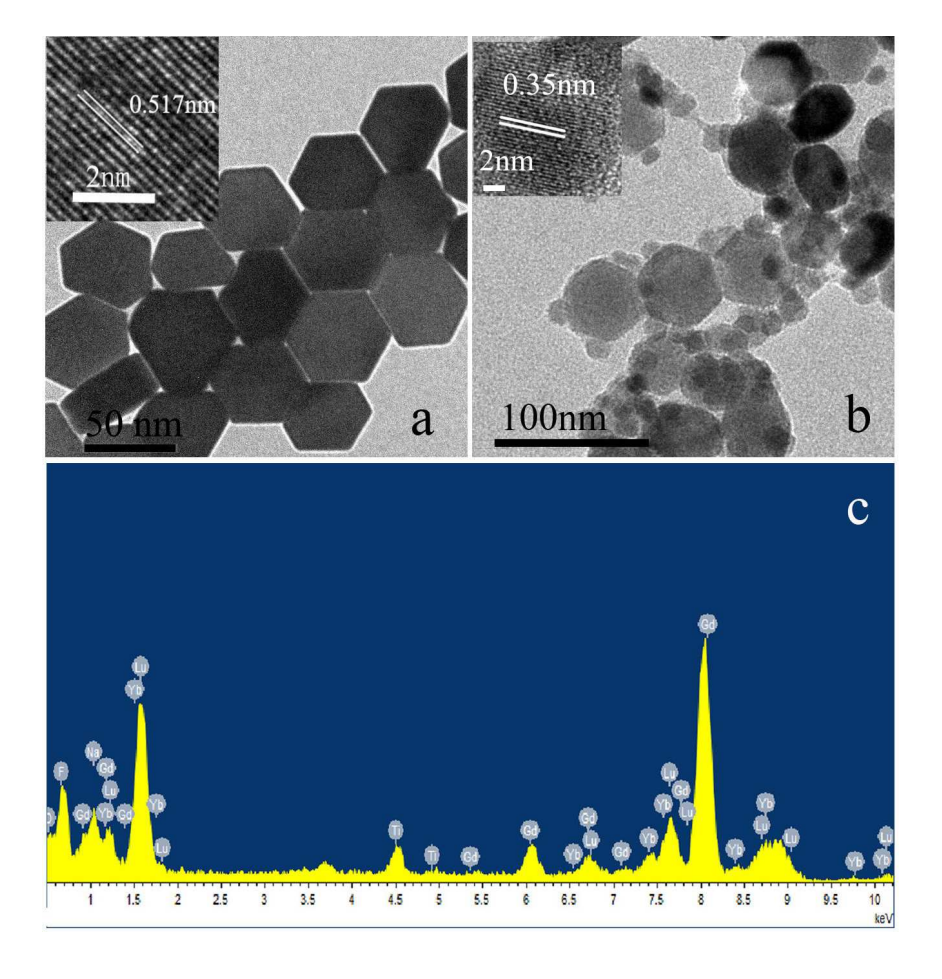


Figure 2. TEM (a) and HRTEM (a, inset) images of NaLuF₄: Gd, Yb, Tm nanocrystals, TEM (b) and HRTEM (b, inset) images of NaLuF₄: Gd, Yb, Tm/TiO₂ nanocomposite and TiO₂, and EDX spectrum of the NaLuF₄: Gd, Yb, Tm/TiO₂ nanocomposite (c).

3.2. UV-vis-NIR absorption spectra analysis

UV-vis-NIR absorption spectra of NaLuF₄: Gd, Yb, Tm nanocrystal and NaLuF₄: Gd, Yb, Tm/TiO₂ nanocomposite are shown in Figure 3. Both of the products have an absorption peak at 980 nm which is attributed to the absorption of Yb³⁺ ions, ^{23,26} while the nanocomposite has sharp peaks emerging at ~400 nm corresponding to the bandgap absorption of TiO₂. ¹⁵ Based on the UV-vis-NIR spectra, it can be speculated that the UV photos generated from the

upconversion process of NaLuF₄: Gd, Yb, Tm can be absorbed by the anatase TiO₂ via an energy transfer.

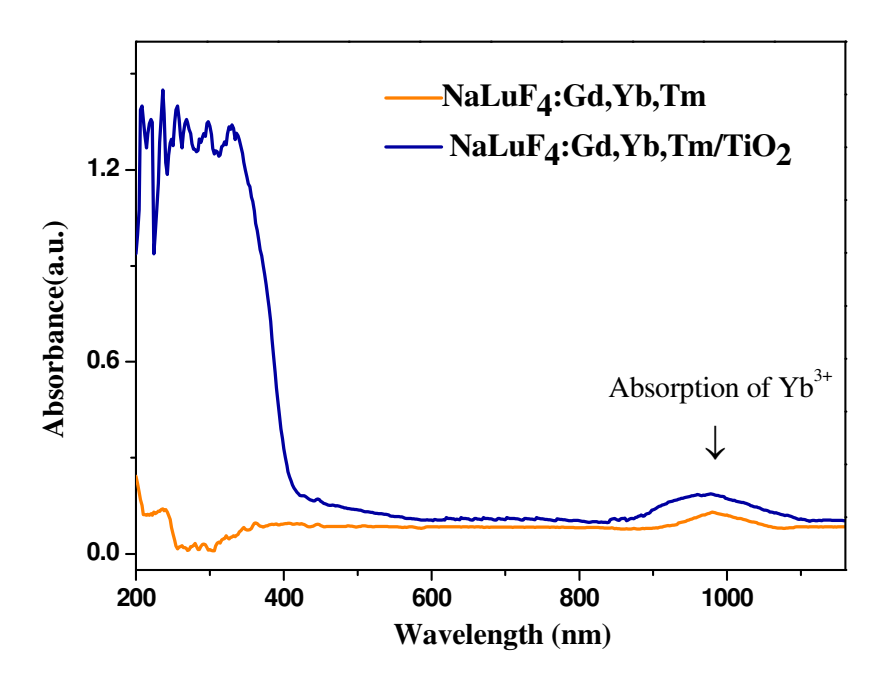


Figure 3. UV-vis-NIR absorbance spectra of NaLuF₄: Gd, Yb, Tm nanocrystal and NaLuF₄: Gd, Yb, Tm/TiO₂ nanocomposite.

3.3. Upconversion luminescence properties of the nanocomposite

The upconversion luminescenne properties of the as-prepared products are investigated. As shown in Figure 4, Under a 980 nm laser excitation, NaLuF₄: Gd, Yb, Tm emits UV and blue lights, where UV emission peaks centered at 291, 349, and 362 nm are attributed to the transitions of Tm³⁺ ions: ${}^{1}I_{6} \rightarrow {}^{3}H_{6}$, ${}^{1}I_{6} \rightarrow {}^{3}F_{4}$, and ${}^{1}D_{2} \rightarrow {}^{3}H_{6}$, respectively. 23,26 Two blue emissions at 450 nm and 478 nm are assigned to ${}^{1}D_{2} \rightarrow {}^{3}F_{4}$ and ${}^{1}G_{4} \rightarrow {}^{3}H_{6}$ transitions of Tm³⁺ ions, respectively. 23 The emission at 314 nm is originated from the ${}^{6}P_{7/2} \rightarrow {}^{8}S_{7/2}$ transitions of

Gd³⁺.²⁷ For the large energy gap between the ground state ⁸S_{7/2} and the first excited state ⁶P_J, the Gd³⁺ cannot absorb 980 nm photons directly. However, the excited states ⁶I_I of Gd³⁺ can be populated through the ET $^3P_2 \rightarrow ^3H_6$ (Tm $^{3+}$): $^8S_{7/2} \rightarrow ^6I_J$ (Gd $^{3+}$). 27,28 At room temperature, the nonradiative relaxation probability of ${}^6I_J \rightarrow {}^6P_J$ is larger than the radiative transition probability of $^6I_{7/2} \rightarrow {}^8S_{7/2}$, which results in populating $^6P_{5/2}$ and $^6P_{7/2}$ levels. 28 So the nonradiative decay ${}^6I_J \rightarrow {}^6P_J$ results in ${}^6P_J \rightarrow {}^8S_{7/2}$. Furthermore the doped Gd^{3+} can promote the phase transformation of nanocrystals from cubic to hexagonal phases, ²⁹ resulting in high upconversion luminescence since the upconversion luminescence of hexagonal phase nanocrystals is higher than that of cubic phase. 19 It is noticeable that strong UV light is obtained in NaLuF₄: Gd, Yb, Tm upon NIR excitation, which can be absorbed by TiO₂ and promote the photocatalytic activity of TiO₂ subsequently. As shown in Figure 4, the spectrum of nanocomposite NaLuF₄: Gd, Yb, Tm/TiO₂ is different from NaLuF₄: Gd, Yb, Tm, where the emission peak at 291 nm nearly disappears, and the emission intensities at 314, 349, and 362 nm decrease obviously. The decrease of emission intensities can be attributed to the energy transfer between NaLuF₄: Gd, Yb, Tm and TiO₂. The emissions at 450 and 478 nm were unchanged, indicating the TiO₂ only absorbs the UV light. In contrast, although the emission intensities in 291, 314, 349, and 362 nm for NaLuF₄: Gd, Yb, Tm-TiO₂ physical mixture also decrease, the decreasing is less than that of the nanocomposite. This can be assigned to the different energy transfer efficiencies. For nanocomposite, NaLuF4: Gd, Yb, Tm and TiO₂ attach closely to each other and form compact interfaces, which benefit energy transfer processes.²³ In contrast, there are no contact interfaces between NaLuF₄: Gd, Yb, Tm and TiO₂ particles in the physical mixture, thus the energy transfer is more difficult than that of the nanocompoiste.²³

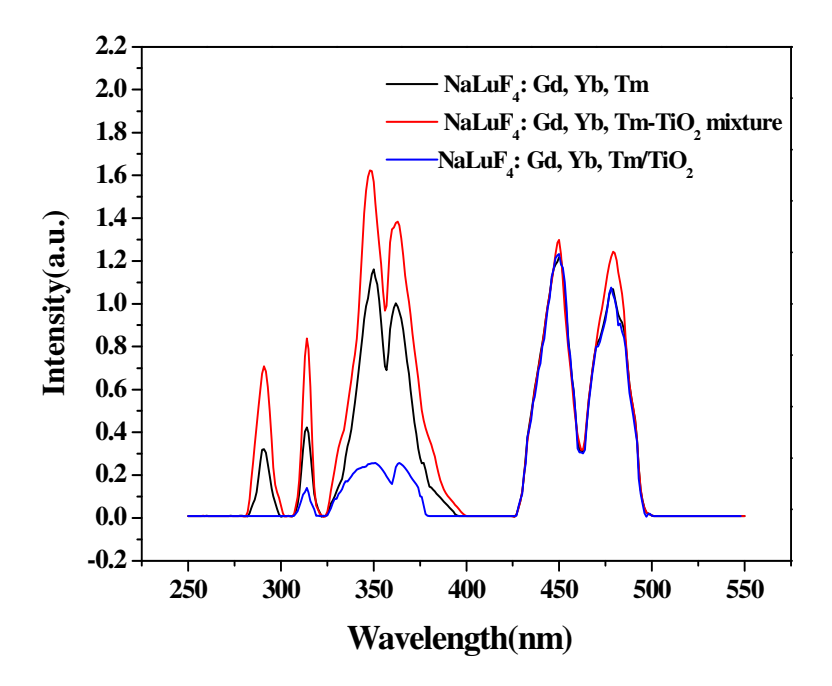


Figure 4. Upconversion luminescent spectra of NaLuF₄: Gd, Yb, Tm, NaLuF₄: Gd, Yb, Tm/TiO₂ nanocomposite, and NaLuF₄: Gd, Yb, Tm-TiO₂ physical mixture under 980 nm excitation

3.4. Photocatalytic measurements

Firstly, RhB was used as a model pollutant to investigate the photocatalytic activity of NaLuF₄: Gd, Yb, Tm/TiO₂ nanocomposite. A 500 W xenon lamp (wavelength distribution: 300-2500 nm) was used as simulated solar light for light source. Upon irradiation for a designated time, 3 mL RhB aqueous solution was taken out for absorbance measurement. Figure 5a shows the absorbance spectra of RhB catalyzed by the NaLuF₄: Gd, Yb, Tm/TiO₂ nanocomposite under simulated solar light irradiation as a function of the irradiation time. The absorption intensity of RhB at 554 nm decreases gradually with the increase in the

irradiation time, indicating the degradation of RhB upon the solar light irradiation. The photocatalytic efficiency of the nanocomposite can be evaluated through calculating the time-depended degradation ratio of dye with contrast in blank, P25, TiO₂, NaLuF₄: Gd, Yb, Tm nanocrystal and NaLuF₄: Gd, Yb, Tm-TiO₂ physical mixture. It can be seen from Figure 5b, the photocatalytic activity of NaLuF₄: Gd, Yb, Tm/TiO₂ nanocomposite is obviously higher than that of controls. The blank test confirms that RhB is quite stable. When catalyst is absent, no obvious change of RhB concentration is observed after irradiation for 250min. The similar result is observed for using NaLuF₄: Gd, Yb, Tm as catalyst, indicating NaLuF₄: Gd, Yb exhibits no catalytic activity. The RhB is almost completely degraded (98.76%) in the presence of NaLuF₄: Gd, Yb, Tm/TiO₂ under the illumination of Xe lamp for 250min, whereas the degradation ratios of NaLuF₄: Gd, Yb, Tm-TiO₂ physical mixture, P25 and TiO₂ are only 58.9%, 33.6% and 27.3% respectively. The photocatalytic activity of NaLuF₄: Gd, Yb, Tm/TiO₂ nanocomposite is about 1.7 times higher than that of NaLuF₄: Gd, Yb, Tm-TiO₂ physical mixture, which can be assigned to the difference in their energy transfer efficiencies discussed above. There are no contact interfaces between NaLuF₄: Gd, Yb, Tm and TiO₂ particles in the physical mixture, thus the energy transfer efficiency is lower than that of the nanocompoiste.²³ In comparison with commercial P25 which is a well-known benchmark catalyst, and pure TiO₂, the photocatalytic activity of NaLuF₄: Gd, Yb, Tm/TiO₂ nanocomposite is remarkably higher (~2.9 and 3.6 times), demonstrating that the as-prepared nanocomposite that composed with NaLuF4: Gd, Yb, Tm and TiO2 can significant improve the photocatalytic activity of pure TiO₂. It is worth to note that the photocatalytic efficiency of the nanocomposite is higher than the ones reported in the literatures. 15,16,22,23

As shown in Figure 6, the photocatalytic degradation of RhB catalyzed by the prepared samples fits a first-order reaction kinetics well, that is, $-\ln(C/C_0) = kt$, where k is the apparent rate constant. In our experiment, k is found to be 1.541×10^{-2} , 3.75×10^{-3} and 1.71×10^{-3} min⁻¹ for NaLuF₄: Gd, Yb, Tm/TiO₂ nanocomposite, NaLuF₄: Gd, Yb, Tm-TiO₂ physical mixture and P25, respectively. The degradation rate of NaLuF₄: Gd, Yb, Tm/TiO₂ nanocomposite is about 9 times higher than that of P25. The high rate constant of NaLuF₄: Gd, Yb, Tm/TiO₂ further confirmed its high photocatalytic activity.

The adsorption of catalysts to contaminant molecules may affect the photocatalytic efficiency. Hence the adsorption levels of the samples for RhB were measured. As shown in Figure 7, after 30 min dark adsorption under stirring, the concentrations of RhB remaining in solution are almost equal for different catalysts, indicating the adsorption ability of the prepared NaLuF₄: Gd, Yb, Tm/TiO₂ nanocomposite catalyst is almost the same as others, indicating that the higher catalytic activity of it is not caused by physical adsorption.

The influence of the catalyst amount on the photocatalytic degradation of RhB was investigated by varying the amount of catalyst NaLuF₄: Gd, Yb, Tm/TiO₂ from 5 to 55 mg. Figure 8 shows the changes of degradation ratios along with various amount of catalyst. The degradation ratio increases lineally as the increase of the catalyst amount in low concentration region, but decreases as the amount reaches to 20 mg. It implies that an optimized amount of catalyst is necessary for enhancing the degradation ratio. The redundant catalysts can enhance light reflectance and decrease light penetration.³⁰

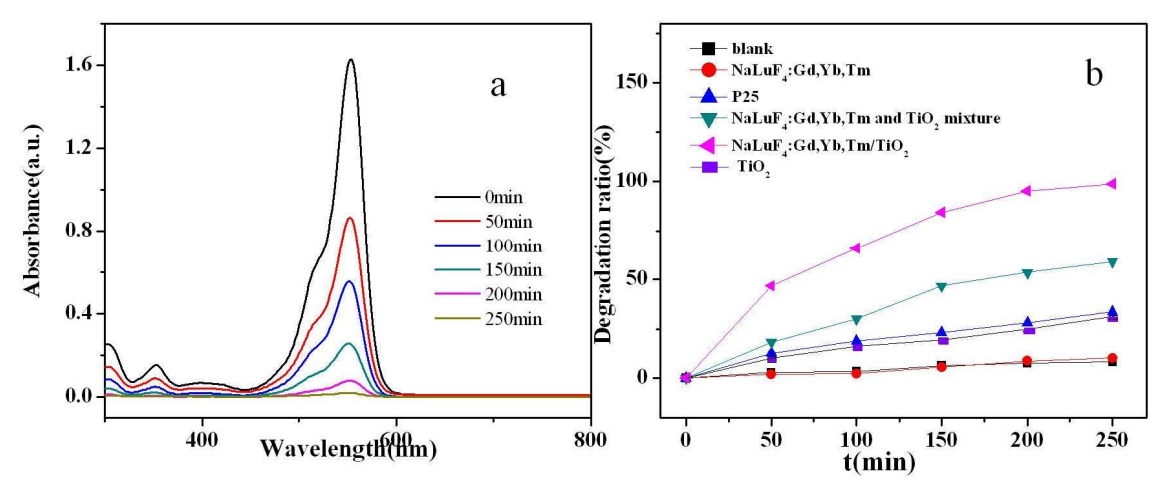


Figure 5. Absorbance spectra of RhB catalyzed by the NaLuF₄: Gd, Yb, Tm/TiO₂ nanocomposite at different irradiation times under simulated solar light irradiation (a); photocatalytic degradation of RhB under simulated solar light irradiation(b).

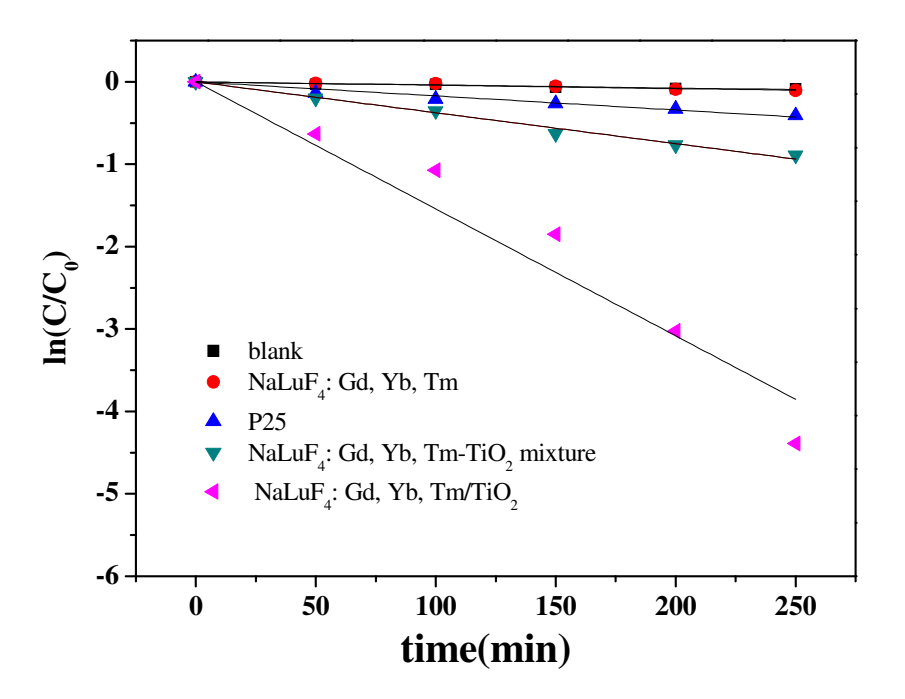


Figure 6. Kinetics of RhB degradation under solar light irradiation

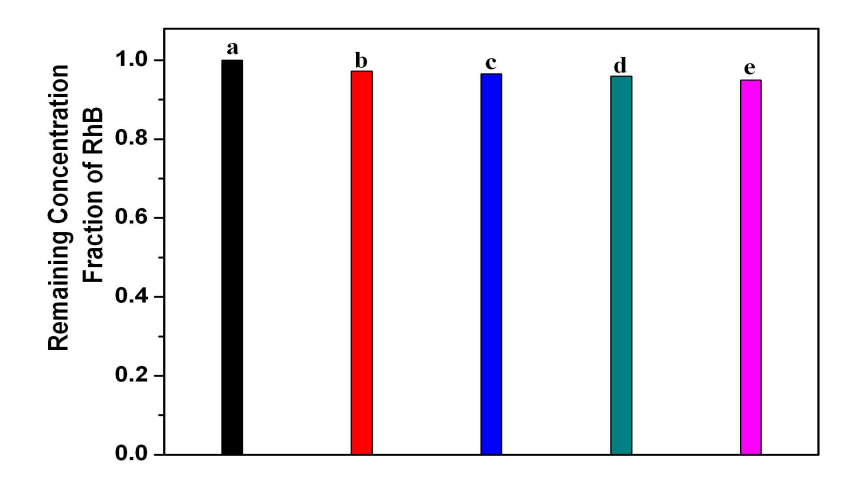


Figure 7. Bar plot showing the remaining RhB in solution: (a) initial and equilibrated with (b) P25, (c) NaLuF₄: Gd, Yb, Tm, (d) NaLuF₄: Gd, Yb, Tm-TiO₂ physical mixture, (e) NaLuF₄: Gd, Yb, Tm/TiO₂ nanocomposite.

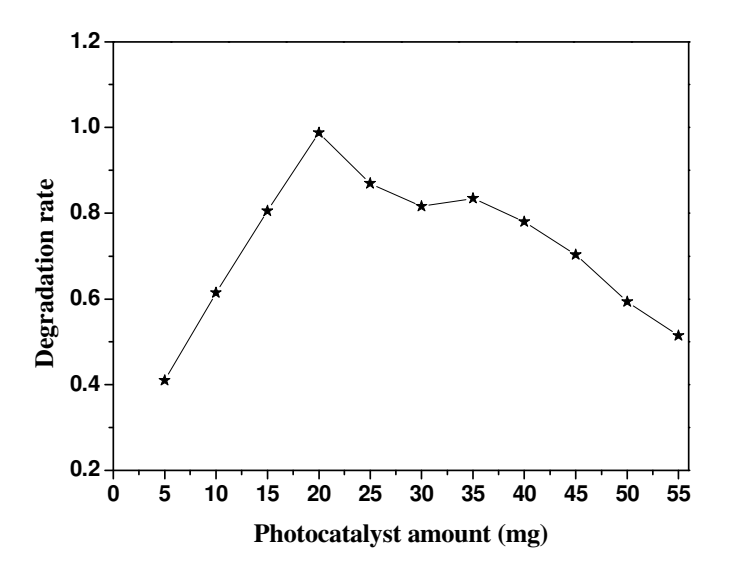


Figure 8. Influence of catalyst loading on the degradation of RhB under simulated solar light ([RhB]= 10 mg/L, t=250min).

The photocatalytic activity of the prepared catalyst was also evaluated through photocatalytic degradation of MB and MO. As shown in Figure 10, after illuminating the samples under Xe lamp for 250min, the degradation ratios of MB and MO are 95.5% and 82.9%, respectively, In contrast, when P25 was used, the degradation ratios of MB and MO

are 48.6% and 45.3%. These results demonstrate that the prepared catalyst can be used for the degradation of MB and MO as well. However, it needs to be noted that their degradation ratios are different under the same photocatalytic condition. This can be attributed to the different molecule structures of the dyes considering that the photodegradation of dyes depends on the structure and anchoring group of the dyes as well. The molecule structures of RhB, MB and MO are shown in Figure 9. In general, benzene ring has the best stability and anthracene ring has the worst stability. Thus MO is more reluctant to photodegradation compared with the other two dyes. Structure with carboxylate as electron donor is favorable for the degradation reaction, the RhB is comparative easy to be degraded.

$$(H_5C_2)_2N$$

$$(H_5C_2)_2N$$

$$(H_3C)_2N$$

$$(H_3C)_2N$$

$$Methylene blue (MB)$$

$$(MB)$$

$$(H_3C)_2N$$

$$Methylene blue (MB)$$

$$(MB)$$

Figure 9. Structure formulas of RhB, MB, and MO

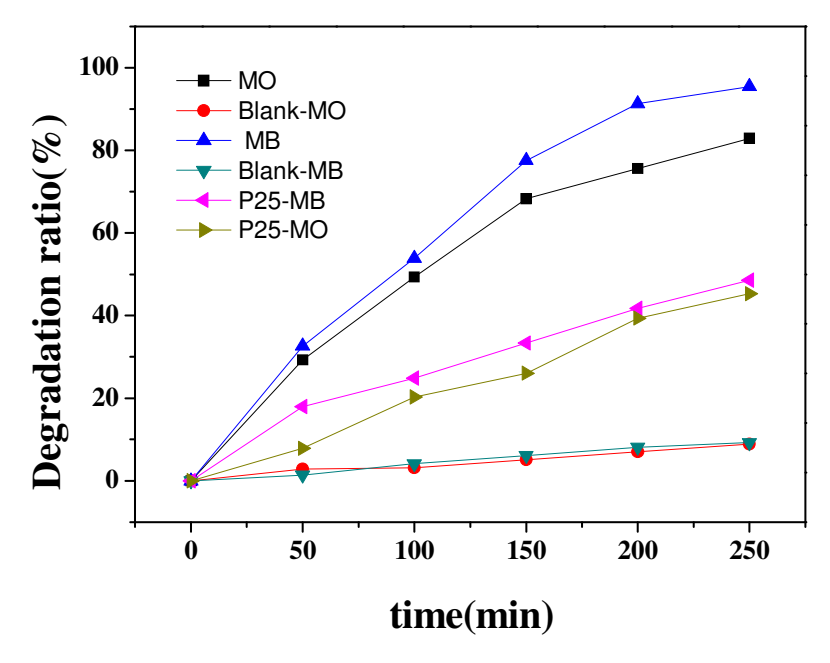


Figure 10. photocatalytic degradation of MB and MO under simulated solar light irradiation

In order to evaluate the mineralization extent of the dyes by photocatalysis, we further measured the chemical oxygen demand (COD) values and COD removal ratios of the dyes. The COD test measures the total quantity of oxygen required for the oxidation of organic matter to small species such as inorganic small molecules of CO₂ and water. Hence it can be used to evaluate mineralization extent of dye.^{34,35} We measured the COD removal ratios of each dyes RhB, MB and MO, dye mixture that consist of equivalent RhB, MB and MO, and a dye wastewater sample taken from a textile printing factory. For all samples, the COD value of photocatalyzed solution was substantially reduced in contrast to that of the initial sample solution. As shown in Figure 11, after treating with catalyst NaLuF₄: Gd, Yb, Tm/TiO₂ under simulated solar light irradiation for 250 min, the COD removal ratios of RhB, MB, MO, dye mixture and dye wastewater are 77.5%, 75.4%, 63.5%, 56.3% and 44.7%, respectively. These results indicate that large part of organic compounds was degraded to inorganic compound. It can be anticipate that, as the increase in irradiation time, the mineralization extent of dye and

wastewater can be further elevated.

Furthermore, the active photo-induced radicals have been determined by collecting radical trapping results in the presence of different radical scavengers. In this study, three chemicals of p-benzoquinone (BZQ, a O_2^- radical scavenger), disodium-ethylenediaminetetraacetate (Na₂-EDTA, a hole scavenger) and *tert*-butanol (a \cdot OH radical scavenger) were employed. The experimental results (Figure 12) show that when Na₂-EDTA scavenger for h⁺ is added to the reaction system, the photodegradation is greatly restrained compared to the reaction without radical scavengers, and the photocatalytic activity is obviously reduced when the BZQ scavenger for \cdot O₂⁻ is added to the reaction system. Whereas, the presence of *tert*-butanol has no obvious effect on the photocatalytic activity. These results imply that h⁺ and \cdot O₂⁻ are the main active species for the photocatalytic reaction.

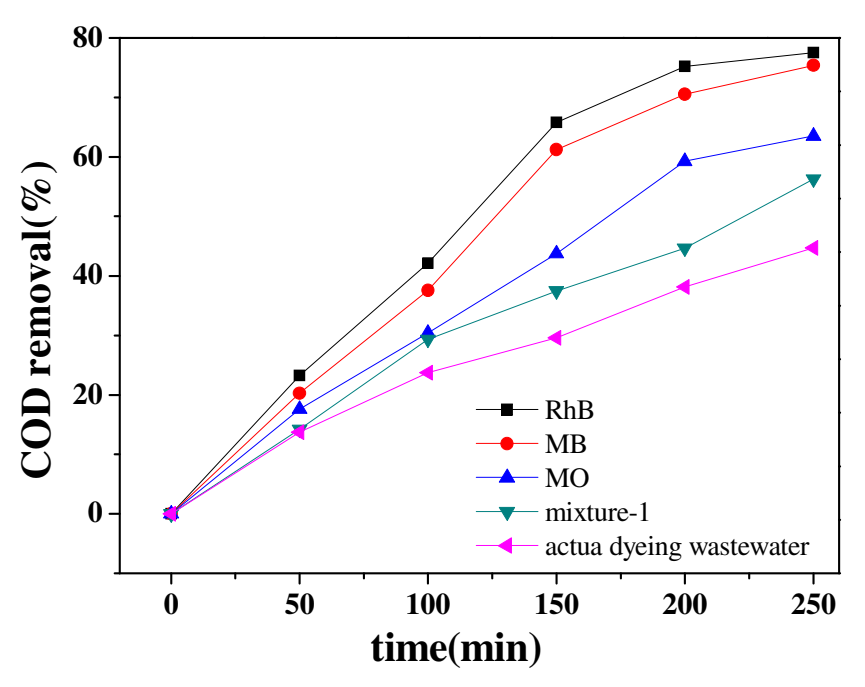


Figure 11. COD removal of dyes under simulated solar light irradiation

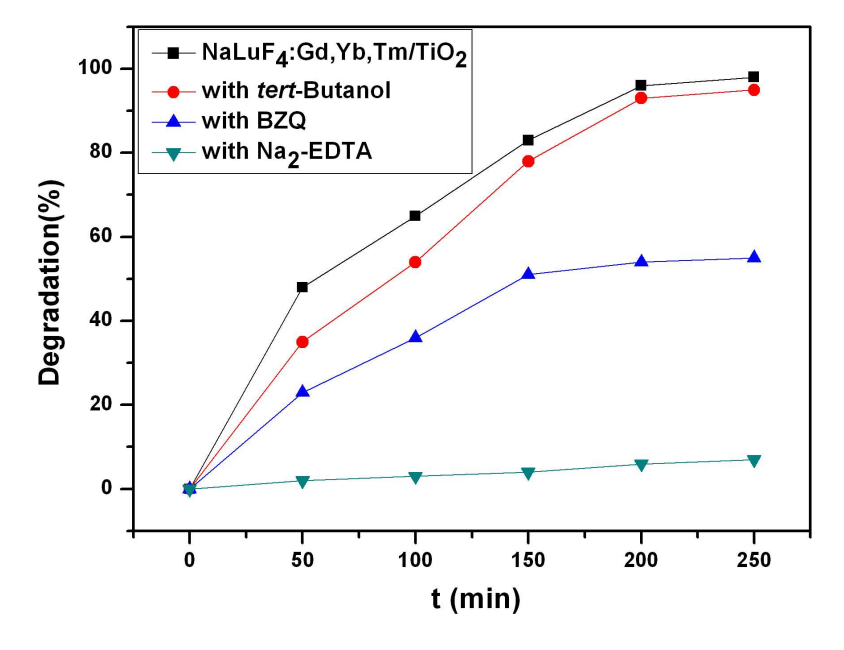


Figure 12. Photocatalytic degradation ratio of RhB using different radical scavengers under simulated solar light irradiation

3.5. Mechanism

As schematic shown in Figure 13, the upconversion nanocrystal of NaLuF₄: Gd, Yb, Tm absorbs energy from the solar lights and upconverts them into UV light emission, which can be absorbed by TiO_2 and generate high energy electrons and holes in the conduction band (CB) and the valence band (VB). These electron-hole pairs then migrate from inner region to the surfaces and act as the catalytic centre. These holes and electrons having high oxidative and reductive abilities can not only directly decompose the organic dye, but also degrade the organic dye indirectly through \cdot OH and \cdot O₂ radicals that are produced from oxidizing H₂O molecules and reducing O₂ molecules by the holes and electrons, respectively.²³

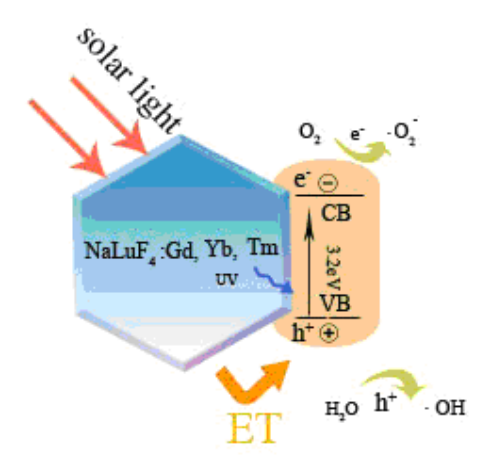


Figure 13. Illustrative diagrams of energy transfer process between NaLuF₄: Gd, Yb, Tm and TiO₂, and the generation of \cdot OH and \cdot O₂ radicals.

4. Conclusions

In this paper, a novel NaLuF₄: Gd, Yb, Tm/TiO₂ nanocomposite photocatalyst was synthesized. The hexagonal-phase nanocrystals NaLuF₄: Gd, Yb, Tm were prepared by a solvothermal method firstly, the small-sized anatase TiO₂ nanoparticles were then attached on NaLuF₄: Gd, Yb, Tm nanocrystals via a hydrolysis and a hydrothermally annealing. Its photocatalytic activity was investigated via photocatalytic degradation of RhB, MB, MO, dye mixture and dye wastewater under the simulated solar light irradiation. The degradation ratios and the COD removal ratios of the dyes and wastewater were measured. In comparison to the pure TiO₂ and P25, the photocatalytic activity of the composite catalyst has been substantially improved. Overall, this report presents an approach to enhance the solar light harvesting ability of TiO₂ based catalytic materials. Considering the catalytic activity of the nanocomposite to real-life wastewater, it can be expected that the prepared product is

potential to be used for environmental cleaning.

Acknowledgments

The authors acknowledge the National Natural Science Foundation of China (No. 21271126, 11025526), National 973 Program (No.2010CB933901), and Program for Innovative Research Team in University (No. IRT 13078).

Notes and References

- 1 M. S. Dresselhaus and I. L. Thomas, *Nature*, 2001, **414**(6861): 332-337.
- M. G. Walter, E. L. Warren, J. R. McKone, S. W. Boettcher, Q. X. Mi, E. A. Santori and N. S. Lewis, *Chem. Rev.*, 2010, 110(11): 6446-6473.
- 3 X. Yang, J. Qin, Y. Li, R. Zhang and H. Tang, *Journal of hazardous materials*, 2013, 261, 342-350.
- 4 X. Yang, J. Qin, Y. Jiang, R. Li, Y. Li and H. Tang, *RSC Advances*, 2014, 4(36), 18627-18636.
- 5 H. Tang, D. Zhang, G. Tang, X. Ji, W. Li, C. Li and X. Yang *Ceramics International*, 2013, **39**(8), 8633-8640.
- 6 G. Tang, S. Liu, H. Tang, D. Zhang, C. Li and X. Yang, *Ceramics International*, 2013, **39**(5), 4969-4974.
- 7 M. Koelsch, S. Cassaignon, C. T. T. Thanh Minh, J. F. Guillemoles and J. P. Jolivet, *Thin Solid Films*, 2004, **451** (542): 86-92.
- 8 G. Liu, Y. N. Zhao, C. H. Sun, F. Li, G. Q. Lu and H. M. Cheng, *Angew. Chem.*, 2008, **47**(24): 4516-4520.
- 9 R. Asahi, T. Morikawa, T. Ohwaki, K. Aoki and Y. Taga, Science, 2001, 293:269-271.
- 10 Y. Izumi, T. Itoi, S. Peng, K. Oka and Y. Shibata, *J. Phys. Chem. C*, 2009, **113**(16): 6706-6718.
- 11 J. L. Zhang, Y. M. Wu, M. Y. Xing, S. A. K. Leghari and S. Sajjad, *Energy Environ. Sci.*, 2010, **3**(6) 715-726

- 12 G. L. Huang and Y. F. Zhu, J. Phys. Chem. C, 2010, 114(3): 1512-1519.
- 13 J. Wang, F. Y. Wen, Z. H. Zhang, X. D. Zhang, Z. J. Pan, P. Zhang, P. L. Kang, J. Tong, L. Wang and L. Xu, *J. Environ. Sci.*, 2005, 17(5): 727-730.
- 14 G. J. Feng, S. W. Liu, Z. L. Xiu, Y. Zhang, J. X. Yu, Y. G. Chen, P. Wang and X. J. Yu, *J. Phys. Chem. C*, 2008, **112** (35): 13692-13699.
- 15 D. G. Yin, L. Zhang, B. H. Liu and M. H. Wu, *J. Nanosci. Nanotechnol.*, 2014, **14**(8): 6077-6083.
- 16 J. K. Zhou, M. Takeuchi, X. S. Zhao, A. K. Raya and M. Anpo, *Catal. Lett.*, 2006, **106** (1): 67-70.
- 17 W. P. Qin, D. S. Zhang, D. Zhao, L. L. Wang and K. Z. Zheng, *Chem. Commun.*, 2010, 46 (13): 2304-2306.
- 18 L. Ren, X. Qi, Y. D. Liu, Z. Y. Huang, X. L. Wei and J. Li, *J. Mater. Chem.*, 2012, **22** (23): 11765-11771.
- 19 D. G. Yin, K. L. Song, J. Ouyang, C. C. Wang, B. Liu and M. H. Wu, *J. Nanosci. Nanotechnol.*, 2013, **13**(6): 4162-4167.
- 20 Q. Liu, Y. Sun, T. S. Yang, W. Feng, C. G. Li and F. Y. Li, *J. Am. Chem. Soc.*, 2011, **133**(43): 17122-17125.
- 21 F. Shi, J. S. Wang and X. S. Zhai, CrystEngComm., 2011, 13(11):3782-3787.
- 22 D. G. Yin, L. Zhang, B. H. Liu and M. H. Wu, *J. Nanosci. Nanotechnol.*, 2012, **12**(2): 937-942.
- 23 Y. N. Tang, W. H. Di, X. S. Zhai, R. Y. Yang and W. P. Qin, *ACS Catal.*, 2013, **3**(3): 405-412.
- 24 H. L. Chen, G. Yang, Y. J. Feng, C. L. Shi, S. R. Xu, W. P. Cao and X. M. Zhang, *Chem. Eng. J.*, 2012, **198**: 45-51.
- 25 A. Xia, M. Chen, Y. Gao, D. M. Wu, W. Feng and F. Y. Li, *Biomaterials*, 2012, **33**(21): 5394-5405.
- 26 J. Zhang, H. O. Shen, W. Guo, S. H. Wang, C. T. Zhu, F. Xue, J. F. Hou, H. Q. Su and Z. B. Yuan, *J. Power Sources*, 2013, 226: 47-53.
- 27 T. Jiang, Y. Liu, S. S. Liu, N. Liu and W. P. Qin, *J. Colloid Interf. Sci.*, 2012, **377**(1): 81-87.

- 28 J. Sytsma, G. F. Imbush and G. Blasse, J. Phys.: Condens. Matter, 1990, 2(23): 5171.
- 29 F. Wang, Y. Han, C. S. Lim, Y. Lu, J. Wang, J. Xu, H. Chen, C. Zhang, M. Hong and X. Liu, *Nature*, 2010, **463**(7284): 1061-1065.
- 30 B. F. Gao, Y. Ma, Y. Cao, W. S. Yang and J. N. Yao, *J. Phys. Chem. B*, 2006, **110**(29): 14391-14397.
- 31 D. Zhao, C. C. Chen, Y. F. Wang, W. H. Ma, J. C. Zhao, T. Rajh and L. Zhang, *Environ. Sci. Technol.*, 2007, **42**(1): 308-314.
- 32 H. Y. Huo, H. J. Su, W. Jiang and T. W. Tan, Biochem. Eng. J., 2009, 43(1): 2-7.
- 33 X. M. Song, J. M. Wu and M. Yan, *Thin. Solid. Films.*, 2009, **517**(15): 4341-4347.
- 34 K. Vignesha, A. Suganthia, M. Rajarajanb and R. Sakthivadivel, *Appl. Surf. Sci.*, 2012, **258**(10): 4592-4600.
- 35 V. K. Gupta, R. Jain, S. Agarwal, A. Nayak and M. J. Shrivastava, *Colloid. Interf. Sci.*, 2012, **366**(1): 135-140.
- 36 X. Yang, H. Cui, Y. Li, J. Qin, R. Zhang and H. Tang, ACS Catalysis, 2013, 3(3), 363-369.
- 37 H. Cui, X. Yang, Q. Gao, H. Liu, Y. Li, H. Tang, R. Zhang, J.Qin and X. Yan, *Materials Letters*, 2013, 93, 28-31.
- 38 X. Yan, Q. Gao, J. Qin, X. Yang, Y. Li and H. Tang, *Ceramics International*, 2013, **39**(8), 9715-9720.